Title: Evaluation of the influence of material properties and process parameters on granule porosity in twin-screw wet granulation

Authors: Michiel Peeters, Ana Alejandra Barrera Jimenez, Kensaku Matsunami, Fanny Stauffer, Ingmar Nopens, Thomas De Beer

Abstract

In recent years, continuous twin-screw wet granulation (TSWG) is gaining increasing interest from the pharmaceutical industry. Despite the many publications on TSWG, only a limited number of studies focused on granule porosity, which was found to be an important granule property affecting the final tablet quality attributes, e.g. dissolution. In current study, the granule porosity along the length of the twin-screw granulator (TSG) barrel was evaluated. An experimental set-up was used allowing the collection of granules at the different TSG compartments. The effect of active pharmaceutical ingredient (API) properties on granule porosity was evaluated by using six formulations with a fixed composition but containing APIs with different physical-chemical properties. Furthermore, the importance of TSWG process parameters liquid-to-solid (L/S) ratio, mass feed rate and screw speed for the granule porosity was evaluated. Several water-related properties as well as particle size, density and flow properties of the API were found to have an important effect on granule porosity. While the L/S ratio was confirmed to be the dictating TSWG process parameter, granulator screw speed was also found to be an important process variable affecting granule porosity. This study obtained crucial information on the effect of material properties and process parameters on granule porosity (and granule formation) which can be used to accelerate TSWG process and formulation development.

Abbreviations

API: Active pharmaceutical ingredient

C: Compartment

CV: Cross-Validation

EQPC: Equivalent projected circle

GSD: Granule size distribution

HPMC: Hydroxypropylmethylcellulose

KZ: Kneading zone

L/D: Length-to-diameter

L/S: Liquid-to-solid

MCC: Microcrystalline cellulose

MFR: Mass feed rate

PBM: Population balance model

PLS: Partial least squares

PSD: Particle size distribution

R^2 :Goodness-of-fit

S: Screw speed

SCE: Size control elements

TSG: Twin-screw granulator

TSWG: Twin-screw wet granulation

UV: Unit variance

1. Introduction

In recent years, continuous manufacturing has been gaining increasing attention from the pharmaceutical industry because of its output flexibility, no need for scale-up, possibility to perform real-time quality control and product diversion (Lee et al., 2015; Rantanen and Khinast, 2015; Vanhoorne and Vervaet, 2020). Twin-screw wet granulation (TSWG) is for some pharmaceutical products a crucial intermediate step in the continuous manufacturing of solid oral drug products to improve the properties of the starting material such as material density, flow, and drug-uniformity.

A thorough understanding of the effect of twin-screw granulator (TSG) process parameters and material properties on granule properties is essential to control the final drug product quality. Porosity was found to be an important granule property affecting the final tablet quality characteristics such as tablet porosity (Badawy et al., 2012), tablet tensile strength (Nordström and Alderborn, 2015), compactability (Badawy et al., 2000; Pandey et al., 2012) and drug release (Ansari and Stepanek, 2008). In addition, porosity is an important property used to physically describe the wet granulation process, in particular granule consolidation behavior (Iveson et al., 1996). Nevertheless, most studies about TSWG investigated the effect of process parameters and material properties on granule attributes such as size, density and friability (Dhenge et al., 2010, 2011, 2012; Vercruysse et al., 2015, 2012; Fonteyne et al., 2013, 2015; Vanhoorne et al., 2016; Meier et al., 2017; Portier et al., 2020a; Ryckaert et al., 2021).

Process models have been developed to simulate granule properties for TSWG (Immanuel and Doyle, 2005, 2005; Poon et al., 2008; Barrasso et al., 2013, 2015; Barrasso and Ramachandran, 2016; Kumar et al., 2016; Van Hauwermeiren et al., 2018, 2020; Liu et al., 2018; Shirazian et al., 2019; Stauffer et al., 2019; Ismail et al., 2019, 2020; Wang et al., 2020; Barrera Jiménez et al., 2021). The application of these models allows to reduce process development time and costs. Recently, a generic one-dimensional population balance model (PBM) was developed predicting granule particle size distribution from raw material properties (Barrera Jiménez et al., 2023a). In order to build generic PBMs predicting granule porosity as well as granule size, the collection of detailed granule property distribution data at intermediate compartments of the TSG is required. However, porosity was only measured for a specific size fraction of the granules at the outlet of the TSG in most of the previous studies (El Hagrasy et al., 2013; Beer et al., 2014; Osorio et al., 2017; Meng et al., 2019). One previous publication evaluated the effect of liquid-to-solid ratio on granule porosity at well-defined compartments inside the TSWG for two model formulations (Verstraeten et al., 2017). The collected porosity data in this study has led to a better understanding of the different physical mechanisms during TSWG for hydrophobic and hydrophilic formulations. The porosity of the agglomerates inside the wetting compartment was found to be lower for the hydrophilic formulation compared to the hydrophobic formulation. This was explained by the higher affinity of the hydrophilic powder particles for the granulation liquid which resulted in more liquid bridges and hence agglomerates with a lower porosity. Nevertheless, the material properties that were responsible for this difference in porosity were not evaluated.

In this study, the effect of raw material properties and process parameters (i.e., L/S ratio, mass feed rate and screw speed) on the granule porosity at intermediate compartments and at the outlet of the TSG were evaluated. The granule porosity for six different formulations with a fixed composition but containing active pharmaceutical ingredients (APIs) with different physical-chemical properties was measured at four intermediate compartments of the TSWG. Linear correlation analysis and partial least squares (PLS) regression were used to quantify the effects of raw material properties and L/S ratio on granule porosity. The objective of this research is therefore to obtain an in-depth understanding of the granule porosity along the length of the TSWG, which is crucial information towards the development of generic PBMs predicting granule porosity from starting material properties.

2. Materials

Six different APIs, 2 fillers and 1 binder were used in this study as listed in Table 1. Some APIs were provided by Janssen Pharmaceutica (Geel, Belgium) and UCB Pharma (Braine-L'Alleud, Belgium). The other APIs were purchased from UTAG (Almere, The Netherlands), Mallinckrodt Pharmaceuticals (Dublin, Ireland), and BASF (Ludwigshafen, Germany). The excipients were purchased from DFE Pharma (Veghel, The Netherlands), Dow Chemical Company (Midland, USA), and FMC BioPolymer (Cork, Ireland). Dry*Flo*® displacement media was obtained from Micromeritics, Norcross, GA.

Table 1 Overview of the used raw materials.

Material	Type	Grade	Supplier	Abbreviation
Hydrochlorothiazide	API	Regular	UTAG	HCT
API 2	API	N/A	Janssen	2_r
API 3	API	N/A	UCB Pharma	3_f
API 4	API	N/A	Janssen	4_r
Paracetamol	API	Dense	Mallinckrodt Pharmaceuticals	P_d
Ibuprofen	API	50	BASF	Ibu
Lactose (Pharmatose)	Filler	200M	DFE Pharma	200M
Microcrystalline cellulose (Avicel) (MCC)	Filler	PH101	FMC BioPolymer	PH101
Hydroxypropylmethylcellulose (Methocel) (HPMC)	Binder	E15	Dow Chemical Company	E15

3. Methods

3.1. Raw material characterization

The powders (Table 1) were characterized to obtain a raw material property database consisting of 51 physicochemical properties of the APIs, fillers and binder (Table 2). A detailed description of the characterization methods can be found in a previous paper from our research group (Ryckaert et al., 2021).

Table 2. Overview of the characterization techniques with their corresponding properties (descriptors) and utilized abbreviations.

Characterization technique	Descriptor	Abbreviation
Laser diffraction using dry and wet ('w') dispersion	10, 50 and 90% cumulative undersize of volumetric particle size distribution (PSD)	d10, d10_w, d50, d50_w, d90, d90_w
	Volume and surface-weighted mean particle size	D[4,3], D[4,3]_w, D[3,2], D[3,2]_w
	Width and span of volumetric PSD	dWidth, dWidth_w, span, span_w
Tapping device	Bulk and tapped density	ρb, ρt
	Compressibility index and hausner ratio	CI, HR
	True density and porosity	ρtrue, ε
Centrifuge	Water binding capacity	WBC
Sessile drop method	Contact angle after 1, 30 and 60 s	CA1, CA30, CA60
Solubility test[1]	Maximum solubility in water	S_{max}
Loss on drying	Moisture content	LoD
Angle of repose test	Angle of repose and cohesion	AoR, SCI
Dissolution test[1]	Fraction powder dissolved after 1', 3', 5', 10', 20', 30' and 60'	DR1, DR3, DR5, DR10, DR20, DR30, DR60
Nitrogen adsorption measurement	Specific surface area	SSA
Ring shear test	Flow function coefficient, unconfined yield stress, major principal stress	ffc, σ_c, σ_1
	Bulk density-weighted flow	ff_{rho}
	linear angle of internal friction, effective angle of internal friction, angle of internal friction at steady state flow	φ_{lin}, φ_e, φ_{sf}
	cohesion	τ_c
	Bulk density	RHOB
Powder rheology: stability and variable flow rate	Basic flow energy, stability index, flow rate index, specific energy	BFE, SI, FRI, SE, CBD
Powder rheology: compressibility	Compressibility at 15 kPa	Cmpr

[1]not measured for microcrystalline cellulose and hydroxypropylmethylcellulose because these swell in water.

3.2. Preparation of granules

The APIs from Table 1 were combined with a fixed excipient base (i.e., 30% Pharmatose, 15% MCC and 5% HPMC) into six different formulations having a drug load of 50% w/w. The use of a fixed composition allowed to evaluate the effect of API properties on granule porosity directly.

Before blending, all APIs were milled using a Quadro U5 Comil (1000 rpm, round holed screen, average hole diameter of 1397 µm, Quadro, Waterloo, Canada) to eliminate possible large agglomerates. Subsequently, all raw materials from each formulation blend were mixed in a tumbling blender (Inversina Bioengineering, Wald, Switzerland) during 15 min at 25 rpm. Granules were then produced using the granulation module of the ConsiGma™-25 unit (GEA Pharma Systems, Wommelgem, Belgium). This granulation module consists of two 25 mm diameter co-rotating screws with a length-to-diameter (L/D) ratio of 20:1. The overview of screw elements is presented in the lowest line of Fig. 1. The blend was fed gravimetrically to the granulation module using a K-tron KT20 loss-in-weight feeder (Coperion K-tron, Niederlenz, Switzerland). Granulation liquid (i.e., demineralized water) was added before the first kneading zone by a twin-peristaltic pump (313VDL/D, Watson-Marlow Fluid Technology Group, Falmouth, UK). The pump was positioned out-off-phase and connected to silicon tubing with an internal diameter of 1.6 or 2.4 mm. The silicon tubes were connected to nozzles with an orifice of 0.8 or 1.6 mm. The selection of nozzles and tubes depended on the liquid flow rate. After wetting, the wetted agglomerates were sheared and compressed in a first kneading zone,

consisting of 6 kneading elements with a L/D of ¼ arranged at an angle of 60°. Granules were further processed in another kneading zone arranged identically to the first kneading zone, after passing a small conveying zone of L = 1.5D. The granules were then transported by a conveying zone (L = 1.5D) towards the end of the granulator. At the end of the screws, three size control elements (SCE) (L = 1D for each size control element) were positioned to reduce the fraction of oversized granules. Before sampling, a stabilisation period was needed to reach steady-state conditions. All collected granules were tray-dried at room temperature (i.e., 25 °C) for 12 hours. Subsequently, the trays were oven dried (40°C, 25% RH) until a moisture content between 1 and 3% was obtained prior to further granule characterization. The moisture content was measured by drying 1 g of material at 105 °C until a stable mass was recorded over a period of 30 s (Mettler Toledo HC103 Halogen Moisture Analyzer, Mettler-Toledo, Zaventem, Belgium).

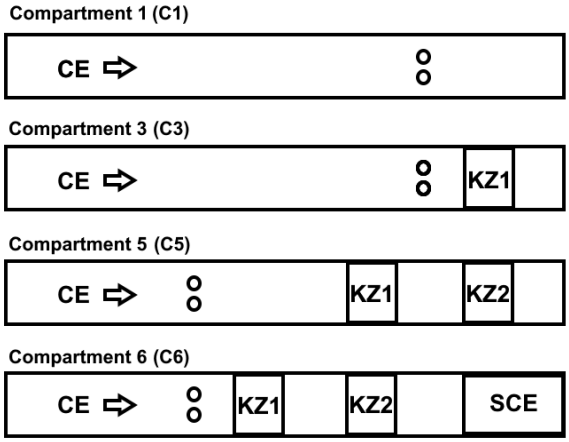

Fig. 1. Experimental set-up of the twin-screw wet granulation experiments. The direction of the powder flow is indicated by the arrow. Screw elements: conveying elements (CE), first kneading zone (KZ1), second kneading zone (KZ2) and size control elements (SCE) . The liquid addition port is represented by the circles.

In order to experimentally characterize the porosity and granule size distribution (GSD) evolution along the length of the granulator barrel, granule samples were collected in well-defined compartments of the twin-screw granulator (TSG) (Fig. 1). This method was described in a previous study by Verstraeten et al. (2017). Granule samples were collected in the following compartments:

- Compartment 1 (C1): Before the first kneading compartment, where the granulation liquid is added (i.e., wetting zone);
- Compartment 3 (C3): After the first kneading compartment;
- Compartment 5 (C5): After the second kneading compartment;
- Compartment 6 (C6): After the size control elements (i.e., granulator outlet).

The first and second kneading zone (i.e., KZ1 and KZ2) represent compartments 2 (C2) and 4 (C4), respectively. By using a second liquid addition port and a screw configuration consisting of only conveying elements, granules collected at the TSG outlet reflect granules in the wetting zone (C1). By placing a kneading zone after the second liquid addition port, granules collected at the TSG outlet represent granules in C3. Samples after the second kneading zone (C5) can be collected at the TSG outlet by using the first liquid addition port and by leaving out the size control elements at the end of the screw configuration.

This method allows to collect large amounts of granules at intermediate TSG compartments (i.e., C1, C3, C5) without the need for a screw pull-out, where only a limited amount of granules (±5 g) can be collected during each experiment (Li et al., 2014).

3.3. Twin-screw wet granulation process conditions

Table 3 shows the overview of process conditions performed in the experiments, where process conditions that were varied are presented in italics. The effect of liquid-to-solid (L/S) ratio upon final granule size and friability has been found to be more important compared to mass feed rate (MFR) and screw speed (S) by different researchers (Verstraeten et al., 2017; Portier et al., 2020b, 2021). Therefore, granules were produced for each formulation applying a low and high L/S ratio, which were determined based on preliminary experiments, while keeping MFR and S constant at 20 kg/h and 675 rpm (Table 3). In order to study the effect of MFR and S on granule porosity at intermediate TSG compartments and on the final granule porosity, granules from formulation 2R50 were produced at center point L/S ratio (i.e., 10.6%), while varying MFR and S from 15 to 25 kg/h and from 450 to 900 rpm, respectively. Formulation 2R50 was selected since API 2_r has physicochemical properties that are lying in between these of the other APIs from Table 1. The last column of Table 3 shows result section number, where corresponding formulations were used for analysis.

Table 3. Overview of the used formulations and the applied process settings during the granulation experiments. The sieve fractions for which the granule porosity was measured is indicated for each formulation.

Formulation	API name	Solubility (USP classification)	L/S (%) ratio	Screw speed (rpm)	Mass feed rate (kg/h)	Sieve fractions (µm)	Corresponding result section
2R50	2_r	Freely soluble	*5.2, 16.0*	675	20.0	>2000, 850-1000, 150–500	4.3, 4.4
2R50	2_r	Freely soluble	10.6	*450, 900*	20.0	>2000, 850-1000, 150–500	4.5
2R50	2_r	Freely soluble	10.6	675	*15.0, 25.0*	>2000, 850-1000, 150–500	4.5
3F50	3_f	Freely soluble	*7.2, 10.0*	675	20.0	>2000, 1000–2000, 850-1000, 500-850, 150–500	4.2, 4.3, 4.4
PD50	P_d	Sparingly soluble	*13.0, 21.0*	675	20.0	850-1000	4.3, 4.4
H50	HCT	Very slightly soluble	*13.6, 23.7*	675	20.0	850-1000	4.3, 4.4
I50	Ibu	Practically insoluble	*18.0, 28.0*	675	20.0	>2000, 1000–2000, 850-1000, 500-850, 150–500	4.1, 4.2, 4.3, 4.4
4R50	4_r	Practically insoluble	*20.0, 28.0*	675	20.0	850-1000	4.3, 4.4

3.4. Granule characterization

3.4.1. Granule size distribution

A dynamic image analyser (QICPIC particle size analyzer, Sympatec, Clausthal-Zellerfeld, Germany) equipped with a vibrating feeding unit and dry dispersion unit was used to measure the granule size distribution. Samples of 10 g were measured in triplicate. The equivalent projected circle (EQPC) diameter was calculated for each particle to derive the 10%, 50% and 90% cumulative under-size volume fraction of the size distribution (d10, d50 and d90).

3.4.2. Granule porosity

Prior to measuring the granule porosity, the samples were sieved in different fractions (i.e., >2000 µm, 1000–2000 µm, 850-1000 µm, 500-850 µm, 150–500 µm) using a Retsch VE 1000 sieve shaker (Haan, Germany). This allowed to evaluate the effect of granule size on granule porosity.

The granule porosity (ε) was calculated from its envelope (ρ_{env}) and true (ρ_{true}) density using eq 1:

$$\varepsilon = \left(1 - \frac{\rho_{env}}{\rho_{true}}\right) x\ 100 \quad [1]$$

Where the true density (ρ_{true}) is defined as the ratio of the mass of a particle to the sum of the volumes of the solid material and closed pores (voids) within the material. The envelope density ($\rho_{env.}$) of a particle is defined as the ratio of the mass of a particle to the external volume of that particle such as would be obtained by tightly shrinking an imaginary film to contain it (Webb, 2001). Hence, this external volume (i.e., envelope volume) is the sum of the volume of the solid material, closed and open pores. The true density (ρ_{true}) of the granules was measured by a helium pycnometer (Accupyc II 1340, Micromeritics, Norcross, GA), with ten purges and ten runs per measurement. The envelope density (ρ_{env}) of the granules was measured using Geopyc (Micromeritics, Norcross, GA). For this measurement, first, a free flowing solid medium (DryFlow®) was placed in a precision cylinder (plunger diameter = 19.1 mm) and subjected to 10 preparation cycles and 3 measurement cycles under a consolidation force of 38N to obtain the zero-volume baseline. Next, around 1 gram of granules was added to the cylinder followed by a repetition of the preparation and measurement cycles. Hence, the beads of the DryFlow® medium will cover the external contour of the granules. The difference between the baseline volume and the measured volume after adding the sample represents the envelope volume of the granules, from which the envelope density could be calculated.

Based on the envelope density (ρ_{env}) and true density (ρ_{true}), the porosity of the granules at the different TSG compartments (i.e., C1, C3, C5 and C6) within the different size classes from Table 3 was calculated using Equation 1. The granule porosity for the size fraction of 850 – 1000 µm was measured for each formulation and used for the evaluation of the effect of API properties, L/S ratio and screw elements on granule porosity (see Sections 3.5 and 4.3) because it is the middle size fraction and part of the yield fraction (150 – 1500 µm).

For one formulation (I50), the envelope density measurement for the granules collected at C6 was repeated six times for the lowest and highest size fractions (i.e., 150-500 µm and and >2000 µm) and three times for the middle size fraction (i.e., 850-1000µm) to evaluate the measurement variability.

3.5. Evaluation method

Two different statistical approaches were taken for analyzing the impact of API properties. For these analyses, data of all formulations with two L/S ratios were used, i.e., rows 1 and 4-8 in Table 3.

3.5.1. Correlation between API properties and granule porosity

In order to evaluate the linear correlation between the individual API properties (x) (n = 51) (Table 2) and granule porosity (y) (see Section 3.4.2), the Pearson correlation coefficient r was calculated using Equation 2:

$$r = \frac{\sum_{i=1}^{n}(x_i - m_x)(y_i - m_y)}{\sqrt{\sum_{i=1}^{n}(x_i - m_x)^2 \sum_{i=1}^{n}(y_i - m_y)^2}} \quad [2]$$

The average API property and granule porosity were defined as m_x and m_y. The correlation coefficient was calculated by correlating the API properties of the formulations (n = 6) with their corresponding granule porosity in the size fraction 850-1000 µm (y). This correlation coefficient was calculated for 51 different material properties (n = 51). Furthermore, the API properties were correlated with the granule porosity at four TSG compartments (i.e., C1, C3, C5 and C6)

and for granules produced at low and high L/S ratio (see Table 3). Hence, 408 (51 x 4 x 2) correlation coefficients were calculated. A two-sided p-value for each Pearson correlation coefficient was calculated to determine the material properties with a significant correlation ($p < 0.05$) with granule porosity. The calculation of the Pearson correlation coefficients was performed using the Python packages (scipy).

3.5.2. Effect of API properties and liquid-to-solid ratio on granule porosity

With the aim of evaluating the effect of the properties of the API and L/S ratio on granule porosity, the data collected from the experiments described in Sections 3.3 and 3.4 were used to train PLS models correlating the properties of the API and the applied L/S ratio (X data-matrix), with the granule porosity in size fraction 850 – 1000 µm (Y data-matrix). Separate PLS models were trained correlating the X data-matrix with the granule porosity at compartment 1 (Y_1 data-matrix), compartment 3 (Y_3 data-matrix), compartment 5 (Y_5 data-matrix), and compartment 6 (Y_6 data-matrix), respectively. The API properties and L/S ratio (X) were pre-treated prior to PLS regression via unit variance (UV) scaling and mean-centering. The initial data-matrix X consisted of 51 API properties (Table 2) and the applied L/S ratio (Table 3). In order to improve predictive accuracy and include only the material characteristics that are relevant, the number of API properties was decreased based on Cross-Validation (CV) during the development of the PLS models. By changing the combination of API properties, the best combination that maximizes the goodness-of-fit (R^2) values in CV for each model was explored. The reduction of API properties was performed using the procedure described in Fig. 2. Only one property was excluded at each round to avoid exclusion of critical material properties. All data using the same formulation were excluded as test data in the CV method to calculate the R^2. Hence, the R^2 value reflects the predictability for new formulations. The number of LVs was varied from one to five and also chosen based on the R^2 value in CV. The PLS models were developed using the Python packages (scikit-learn).

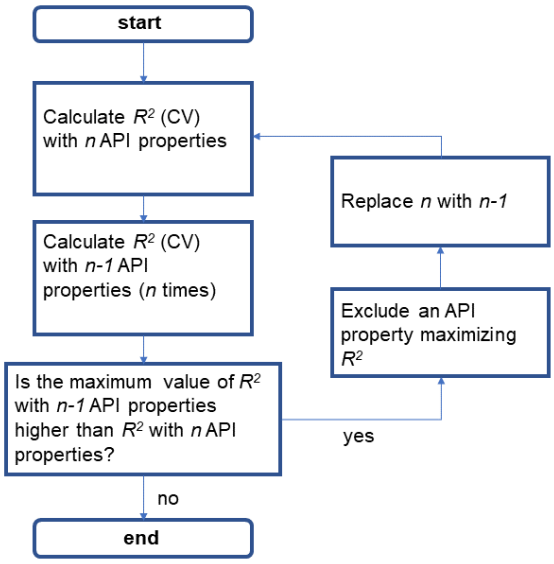

Fig. 2. Workflow used to select the optimal combination of API properties for the PLS models.

4. Results and discussion

4.1. Variability envelope density measurements

The envelope density of the final granules for the size fractions 150 – 500 µm, 850 – 1000 µm and >2000 µm for formulation I50 are shown in Fig. 3. The variability of the Geopyc envelope

density measurements was low as shown by the narrow 95% confidence intervals around the mean envelope density. Subsequently, only one measurement was performed for each size fraction of the remaining experiments from Table 3.

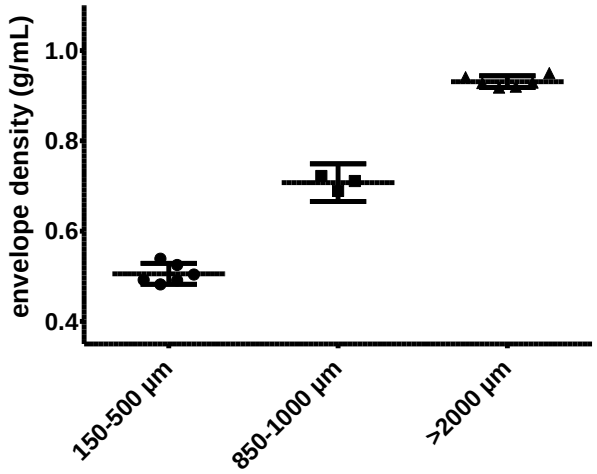

Fig. 3. Envelope density measurements for three sieve fractions of the granules at the granulator outlet (compartment 6 (C6)) of formulation I50. The 95% confidence intervals around the mean envelope density are shown by the vertical error bars.

4.2. Effect of granule size on granule porosity

The granule porosity for five different size fractions (i.e., >2000 µm, 1000–2000 µm, 850-1000 µm, 500-850 µm, 150–500 µm) at each TSG compartment when applying a low and high L/S ratio for formulations 3F50 and I50 is shown in Fig. 4. The granule porosity at each TSG compartment increased with decreasing granule size which can be explained by the lower envelope density of the smaller granules. In the wetting compartment (C1), the reason can be found in the poor liquid distribution among the different granule sizes (El Hagrasy and Litster, 2013). The conveying elements in C1 are not designed to homogeneously distribute the granulation liquid over the powder bed, resulting in the formation of agglomerates with different moisture content. The size of the agglomerates increases with increasing moisture content because particles with a higher moisture content are stronger, more elastic, and hence have less tendency to break into smaller particles. In the large agglomerates that contain a higher amount of binder liquid, powder particles are able to move closer to each other due to the presence of more liquid bridges. Therefore, the interparticle void volume decreases and the porosity decreases. In the kneading compartments and size control elements (C3, C5 and C6), the porosity decreased with increasing granule size likely because of two reasons. First, the porosity of the agglomerates entering the first kneading zone (i.e., agglomerates in C1) decreases with increasing size. Second, large initial granules can only pass the narrow gap (having an estimated size of 400 – 500 µm) between the kneading elements and barrel wall by deforming into elongated, denser particles (Thompson and Sun, 2010). On the other hand, the smaller granules (<500 µm) can pass the kneading zones unaffected and thus their porosity remains unchanged. Larger granules are more densified to be able to pass the space openings and consequently.

At low L/S, there was almost no difference between the porosity of the final granules (C6) and the granules in the wetting compartment (C1) (Fig. 4 – a and c). This might be related to the low liquid pore saturation of granules produced at low L/S ratio, where collisions between granules lead to breakage rather than deformation and consolidation of the initial granules. At high L/S (Fig. 4 – b and d), there was a strong decrease in porosity inside the second kneading zone (KZ2) (i.e., from C3 to C5) of the largest granules (i.e., >2000 µm) because of granule

consolidation by the shear and compression forces of the kneading elements. When using a higher amount of granulation liquid in TSWG, granules have a higher tendency to plastically deform, promoting granule densification (El Hagrasy et al., 2013). The porosity of the smallest granules (150 – 500 µm) for formulation I50 increased when these progress from C3 to C5 (Fig. 4 – c and d) which is unexpected due to the high shear environment in KZ2. For this specific case, the small granules (150 – 500 µm) in C5 could have originated from attrition of the larger granules in KZ2. Outer parts of large granules with a high number of voids (i.e., high porosity) are prone to attrition due to the weak intragranular planes.

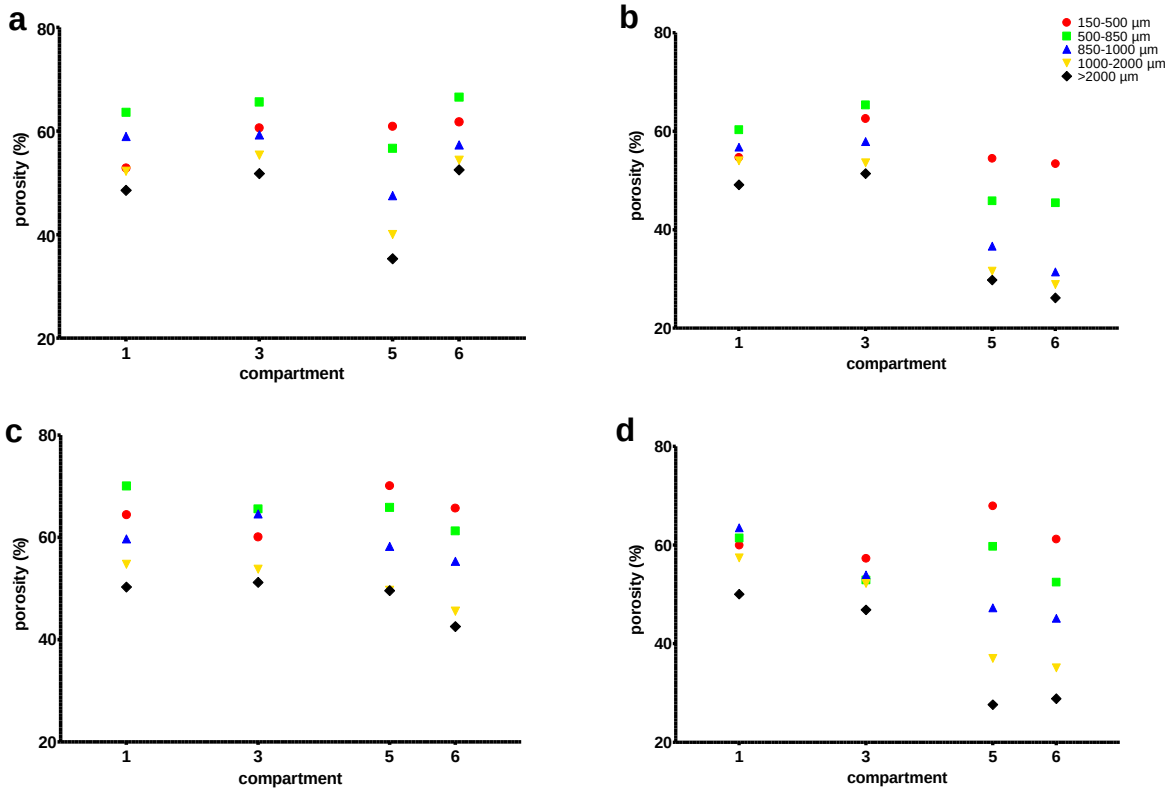

Fig. 4. Granule porosity measured for 3F50 at low (a) and high (b) L/S and for I50 at low (c) and high (d) L/S. Measurements were performed for size fractions 150-500 µm (red), 500-850 µm (green), 850-1000 µm (blue), 1000-2000 µm (yellow) and >2000 µm (black).

4.3. Effect of screw elements on granule porosity

To evaluate the effect of screw elements on granule porosity, the porosity of the granules in size fraction 850 – 1000 µm for the different formulations was compared between the TSG compartments. The granule porosity applying low (a) and high (b) L/S ratio is shown in Fig. 5.

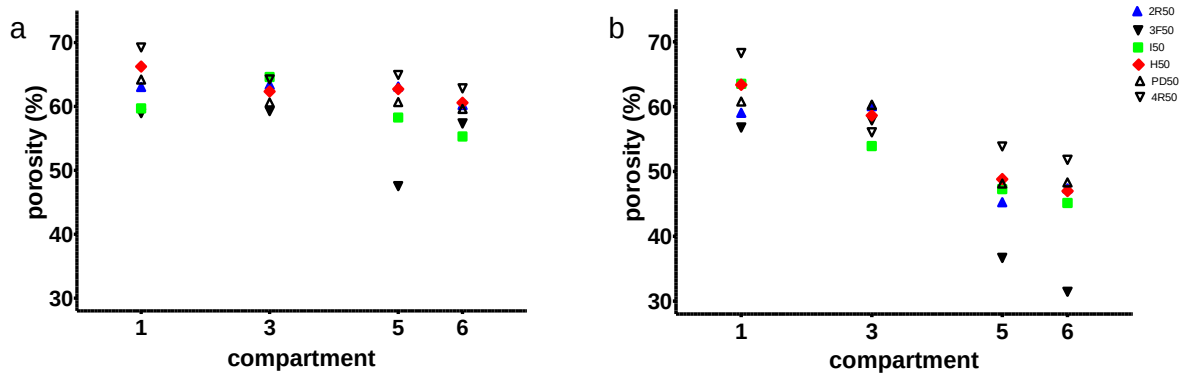

Fig. 5. Granule porosity measured for the different formulations at low (a) and high (b) L/S ratio. Measurements were performed for size fraction 850-1000 µm.

In the wetting compartment (C1), a combination of loose agglomerates and ungranulated powder was obtained, as shown by the very wide granule size distribution in Fig. 6 (a and b). These agglomerates are characterized by a high porosity (C1 in Fig. 5 – a and b) which is related to the lack of shear and compression forces in the wetting compartment.

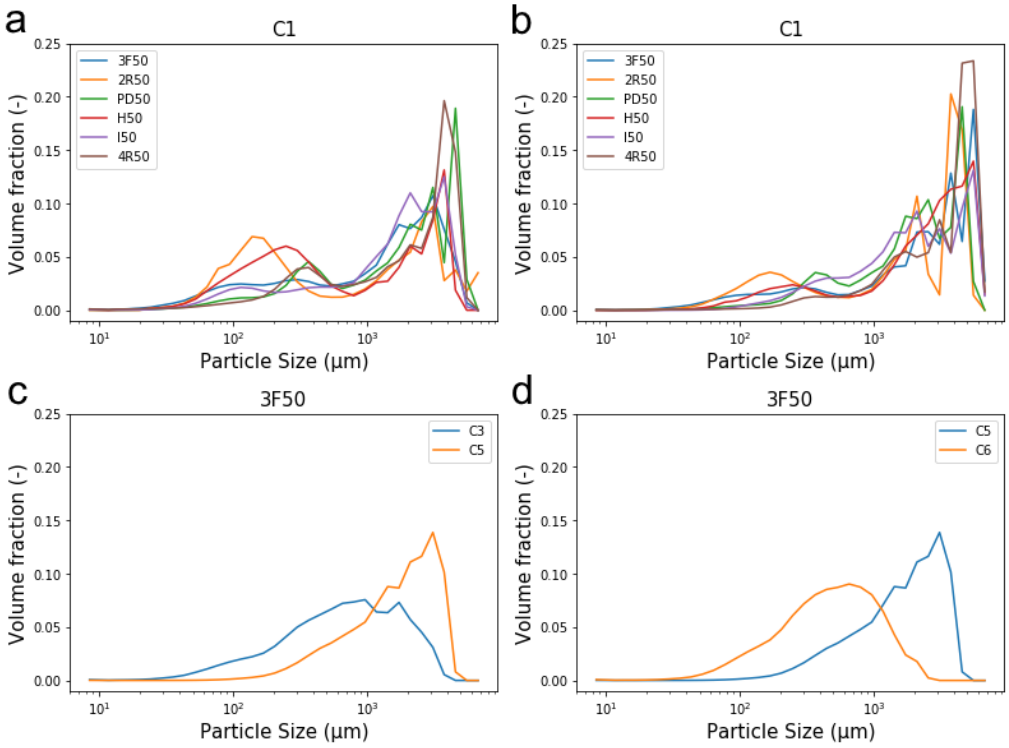

Fig. 6. Granule PSD in C1 at low (a) and high (b) L/S ratio. Change in granule PSD in (c) KZ1 (C3 to C5) and (d) KZ2 (C5 to C6) for 3F50.

The change in granule porosity inside the different kneading zones and SCE was calculated by subtracting the porosity in C1 from the porosity in C3 (i.e., first kneading zone (KZ1)), C3 from C5 (i.e., second kneading zone (KZ2)), and C5 from C6 (i.e., size control elements (SCE)) (Fig. 7).

In the first kneading zone (KZ1), the initial agglomerates are consolidated by compressing the granules between the tip of the kneading discs and the granulator barrel wall. There was a larger reduction in porosity for formulations I50 and 4R50 compared to the other formulations

at high L/S (KZ1 in Fig. 7 – b), which is related to the higher degree of consolidation and densification of the initial agglomerates. The stronger decrease in porosity is caused by the higher amount of granulation liquid applied for these poorly-soluble formulations and thus higher liquid pore saturation compared to other better-soluble formulations. The higher liquid pore saturation increases the particle mobility by acting as a lubricant at inter-particle contact points and thus promotes granule consolidation (Iveson and Litster, 1998).

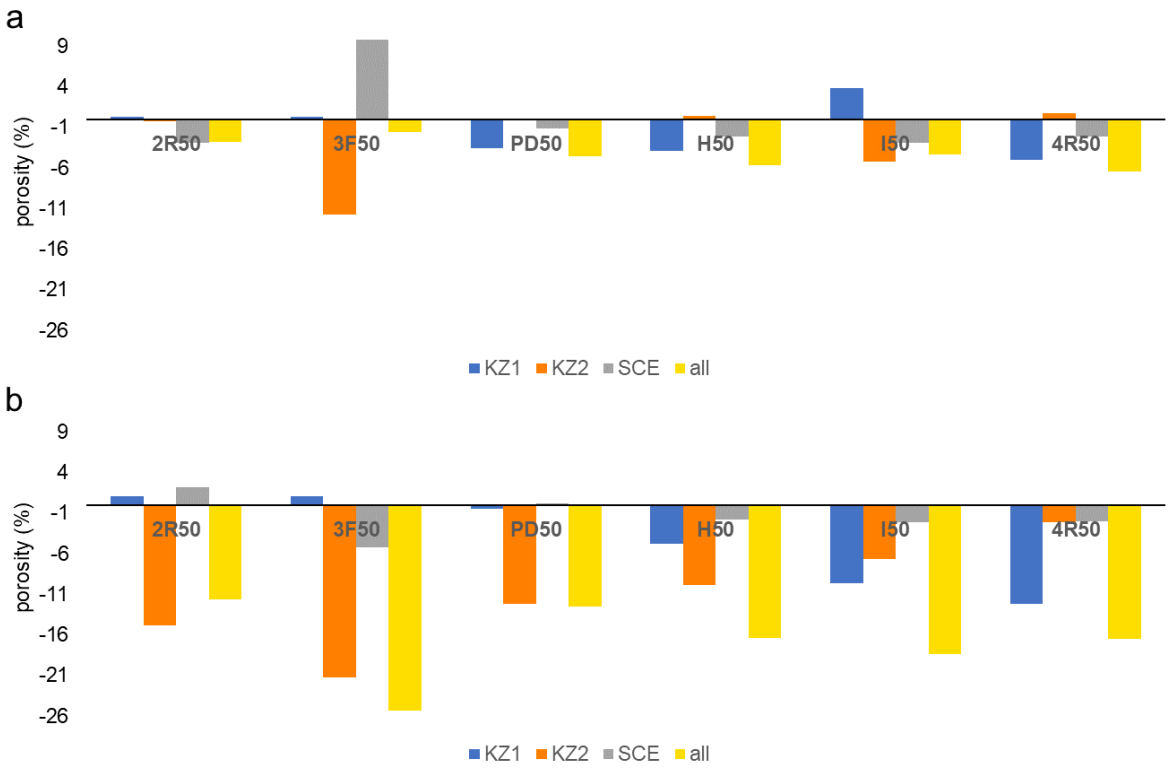

Fig. 7. Change in granule porosity applying low L/S (a) and high L/S (b) in the first kneading zone (KZ1), the second kneading zone (KZ2), the size control elements (SCE) and total change from KZ1 to SCE (all). Formulations are arranged from low to high L/S (from left to right on the x-axis).

Except for formulation 3F50, there was almost no effect on granule porosity in the second kneading zone when using a low L/S ratio (KZ2 in Fig. 7 - a). There was insufficient binder liquid to promote granule densification for most of the formulations. In contrast, because of the high solubility (i.e., S_{max} = 47.61 g/100 mL) and dissolution rate (i.e., DR1 = 2.76%) of 3_f, the amount of dissolved API particles for formulation 3F50 was high. This resulted in granules showing plastic behavior, which led to a strong densification of the initial granules when they passed through the KZ2 (KZ2 in Fig. 7 - a). In addition, this formulation showed a strong increase in granule size in KZ2 (Fig. 6 - c), as the plastic behavior caused granules to expel granulation liquid towards their surface, hence promoting layering of un-wetted powder particles on the granule surface and the coalescence between several granules (Seem et al., 2015; Narang and Badawy, 2019). While the porosity in KZ2 did not change for formulations 2R50 and PD50 at low L/S (Fig. 7 - a), where collisions between granules led to breakage rather than consolidation of the initial granules, their porosity strongly decreased in KZ2 at high L/S (Fig. 7 – b) due to the higher availability of binder liquid.

Only a small decrease in porosity for the formulations containing the APIs with the lowest solubility (I50 and 4R50) at high L/S in KZ2 was observed (Fig. 7 - b). This could be explained by the larger decrease in porosity in KZ1 for I50 and 4R50 compared to the other formulations (Fig. 7 – b), consequently resulting in granules with a lower porosity in C3 (i.e. 53 and 56%,

respectively) (Fig. 5 – b). These dense granules could not be further consolidated by the kneading elements in KZ2.

The granule porosity only slightly changed in the SCE zone, except for formulation 3F50 where the porosity strongly increased at low L/S (Fig. 7 – a). This increase in granule porosity could have two explanations. First, it might be related to breakage of the coarse (>1000 µm) granules into smaller particles due to the weak inter-particle bonds at low liquid feed rate (Fig. 6 - d). The low amount of binder liquid that was applied prevented the formation of numerous strong liquid bridges and hence the granules were weak and easily broke up inside the SCE. The obtained smaller granules were characterized by a higher number of open pores and hence higher porosity. Second, several small and porous granules could have been aggregated into large granules with a low porosity and consequently the porosity for formulation 3F50 decreased inside the SCE. For the other formulations, these results show that the SCE have a smaller impact on granule porosity compared to the kneading elements.

All these results clearly suggest that API properties influence the change in granule porosity inside the granulator barrel. Inside KZ1 at high L/S, the granule porosity only decreased for formulations containing poorly soluble APIs (i.e., I50 and 4R50) because of the consolidation of the initial agglomerates that were obtained in the wetting zone. In contrast, the porosity did not change in KZ1 for several formulations containing well-soluble APIs (i.e., 3F50, 2R50 and PD50), as a lower L/S ratio is applied for these formulations which prevents plastic deformation and granule consolidation. Furthermore, while the porosity decreased at high L/S ratio in KZ2 for well-soluble formulations (i.e., 3F50, 2R50 and PD50) because of plastic deformation of the initial granules, the porosity of poorly-soluble formulations (i.e., I50 and 4R50) remained unaffected due to their lower initial porosity inside C3 of the TSG (Fig. 5 – b).

4.4. Effect of API properties on granule porosity

The effect of API properties on granule porosity at each compartment (i.e., C1, C3, C5 and C6) was determined by calculating the Pearson correlation coefficient R between the raw material properties (n=51) and the granule porosity. The material properties that were significantly correlated ($p < 0.05$) with granule porosity are listed in Table 4.

Size (i.e., d10_w, d50_w, d90_w, D[4,3]_w, dWidth_w) and flow (ffc, τ_c, HR, CI) related properties impacted granule porosity at low L/S ratio and granule porosity was mainly affected by water related properties (i.e., DR, WBC, CA1, S_{max}) when using a high L/S ratio. The granule porosity was not impacted by water related properties at low L/S ratio due to the too limited availability of binder liquid and hence only a small amount of powder being able to dissolve.

Granule porosity increased with increasing API particle size at low L/S ratio, as shown by the positive Pearson coefficients for size related properties (e.g., d50_w, d90_w). The number of inter-particle contact points decreases with increasing API particle size and hence the intra-granular void volume and granule porosity increases. Granule porosity decreased with increasing powder cohesion (i.e., negative Pearson coefficient for τ_c) because of the stronger inter-particle interactions which resulted in a lower granular void volume and thus reduced granule porosity. Powder flowability properties flow function coefficient (ffc) and hausner ratio (HR) were correlated and anti-correlated, respectively, with granule porosity because of their correlation and anti-correlation with particle size. Generally, powders having a larger particle size are also characterized by a better flow (i.e., higher ffc and lower HR). The API solubility (i.e., Smax) and dissolution rate (i.e., DR) were anti-correlated with granule porosity at high L/S ratio because when more powder particles are able to dissolve, more solid bridges are made allowing the individual powder particles to come closer to each other and hence the intra-granular void volume decreases.

Table 4. Material properties showing significant correlation ($p<0.05$) with granule porosity when applying low and high L/S ratio.

	Low L/S ratio			
	C1	**C3**	**C5**	**C6**
Material properties (R, *p*-value)	d50_w (0.887, 0.018) d90_w (0.887, 0.019) D[4,3]_w (0.888, 0.018) dWidth_w (0.880, 0.021) Ffc (0.884, 0.019) τ_c (-0.947, 0.004)	N/A	LoD (-0.817, 0.047)) DR1 (-0.850, 0.032)	d10_w (0.931, 0.007) d50_w (0.939, 0.006) d90_w (0.888, 0.018) D[4,3]_w (0.925, 0.008) dWidth_w (0.847, 0.033) HR (-0.844, 0.035) CI (-0.824, 0.044) τ_c (-0.957, 0.003)
	High L/S ratio			
	C1	**C3**	**C5**	**C6**
Material properties (R, *p*-value)	WBC (0.948, 0.004) CA1 (0.850, 0.032) DR3 (-0.825, 0.043) DR5 (-0.826, 0.043) DR10 (-0.815, 0.048) DR20 (-0.823, 0.044) DR30 (-0.829, 0.042) DR60 (-0.829, 0.041)	Pb (0.883, 0.020)	S_{max} (-0.910, 0.012)) DR1 (-0.923, 0.009) DR3 (-0.879, 0.021) DR5 (-0.833, 0.040) DR30 (-0.821, 0.045) DR60 (-0.825, 0.043)	S_{max} (-0.868, 0.025) DR1 (-0.910, 0.012)

Next, the effect of the material properties as well as liquid-to-solid ratio on the granule porosity at each compartment was evaluated by PLS. While the Pearson correlation analysis quantifies the impacts of material properties on granule porosity at low and high L/S ratio, PLS allows to quantify the overall impact of material properties regardless of the applied L/S ratio. Furthermore, PLS evaluates the effect of material properties on granule porosity compared to that of L/S ratio itself.

The selection of API properties as well as the number of LV of each PLS model was performed by CV. The details of the created PLS models (i.e., number of API properties and latent variables (LV), R^2X, R^2Y, R^2 (CV)) can be found in Table 5. The parameters R^2X and R^2Y represent the percentage of variation of X (API properties and L/S ratio) and Y (porosity) explained by the model, respectively. R^2 quantifies the predictability of the models. The lowest value of R^2X for PLS_{C6} was due to the smaller number of LV used compared to the other models. While R^2 (CV) for PLS_{C3} and PLS_{C6} were relatively lower, the values were high enough for the purpose of the study considering the fact that the common threshold of R^2 (CV) is zero (Götz et al., 2010).

Table 5. Overview of the PLS models built to evaluate the effect of material properties and L/S ratio on granule porosity in C1 (PLS_{C1}), C3 (PLS_{C3}), C5 (PLS_{C5}) and C6 (PLS_{C6}). The number of API properties and LVs used to construct the models as well as the percentage of variation of X (R^2X) and Y (R^2Y) explained by the models and the goodness-of-fit (R^2) calculated by cross validation are listed.

	API properties (n)	LV (n)	R^2X	R^2Y	R^2 (CV)
PLS_{C1}	22	4	0.75	0.87	0.79
PLS_{C3}	11	5	0.96	0.69	0.39
PLS_{C5}	13	4	0.83	0.96	0.85
PLS_{C6}	11	3	0.66	0.69	0.57

The general importance of the API properties and L/S ratio for the granule porosity at each compartment was obtained through the variable importance for the projection (VIP) of the PLS models (Fig. 8). Since empirical evidence from heuristics suggests that a VIP cut-off of around 0.8 is an effective threshold (Eriksson et al., 2013), variables with a VIP score above 0.8 were considered to be important in this study. Overall, similar properties were found to be important for granule porosity compared to the evaluation by Pearson linear regression. The differences in key material properties and effect of L/S ratio upon granule porosity between the intermediate compartments can be assessed by comparing the VIP plots of the different PLS models. Particle size (e.g., d90_w) was important in the wetting zone (C1, Fig. 8 - a) and in compartment 3 (C3, Fig. 8 - b) while it did not have a large effect on porosity in compartment 5 (C5, Fig. 8 - c) and compartment 6 (C6, Fig. 8 - d). This is likely because granules become more densified towards the TSG outlet due to the shear forces of the kneading elements and therefore the effect of the API particle size on the intra-granular void volume became smaller. In addition, water-related properties (e.g., S_{max}, DR1, DR5) were most influential in C5 and C6. This increased importance of water-related properties at C5 and C6 could be explained by the short material residence time in the TSWG process and the effect of the kneading elements on the granules in the intermediate compartments. As the residence time is rather short (i.e., 4-20s (Vercruysse et al., 2012)), only a small fraction of the powder is able to dissolve in the upstream compartments (C1 and C3) and therefore the effect of water related properties upon granule porosity is rather small. In contrast, when the powder blend is transported towards the TSG outlet and intensely mixed with the binder liquid by the kneading elements and SCE, thus allowing a larger fraction of powder particles to dissolve, water-related properties become more important. L/S ratio was found to be more important in compartments C3, C5 and C6 compared to C1 where several API properties (e.g., d90_w, WBC, DR1, SE) were as important as L/S ratio (Fig. 8). The reason can be found in the low-shear environment of the wetting zone (C1). Because the granules are consolidated by the pressure of the kneading elements in the subsequent kneading zones, the effect of the amount of binder liquid and thus inter-particle lubrication on granule porosity becomes larger in these downstream compartments.

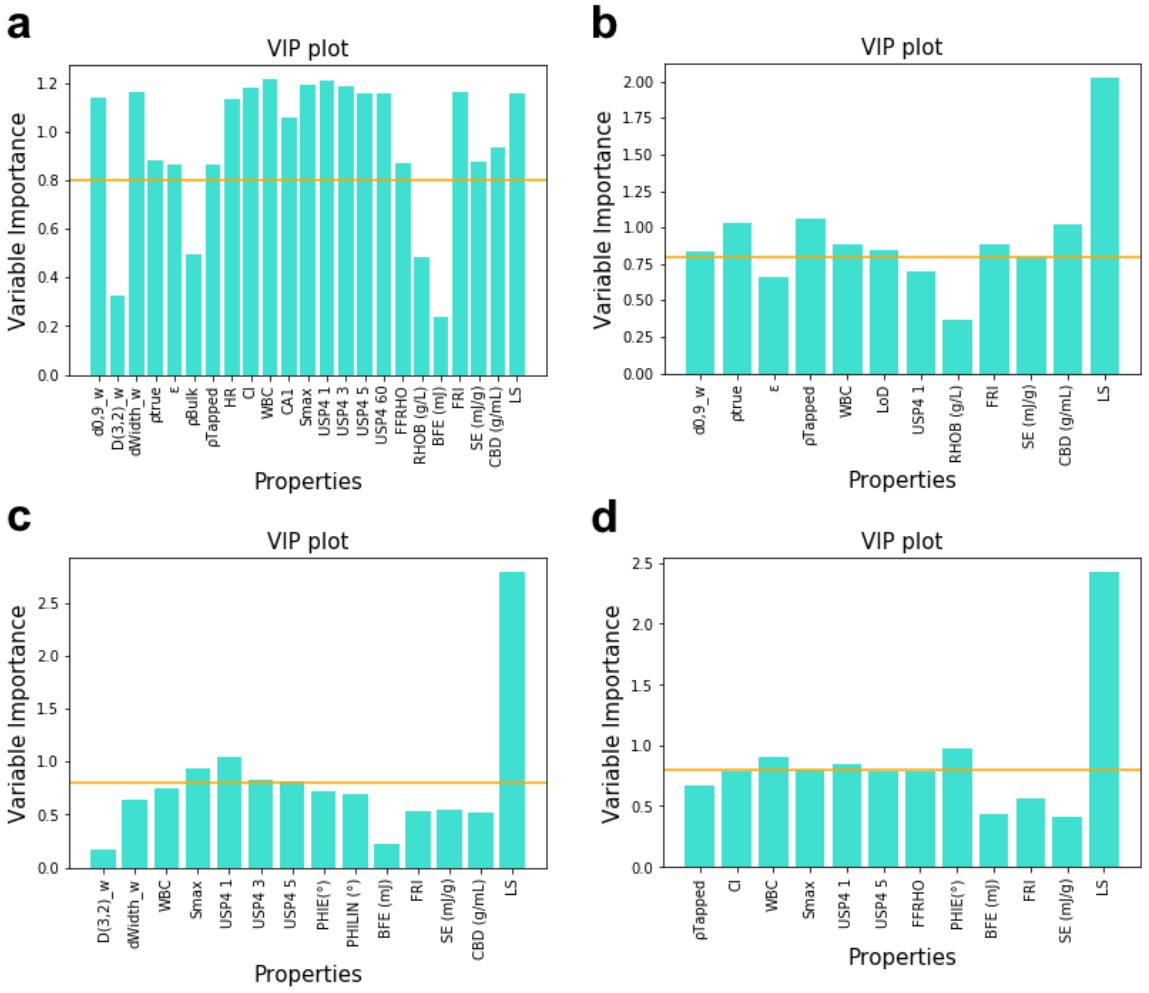

Fig. 8. VIP plots of (a) PLS_{C1}, (b) PLS_{C3}, (c) PLS_{C5} and (d) PLS_{C6}. Variables with a VIP score above 0.8 (yellow horizontal line) were considered to be important.

4.5. Effect of liquid-to-solid ratio, mass feed rate and screw speed on granule porosity

The porosity of the granules collected at each compartment for formulation 2R50 at low and high liquid-to-solid ratio, mass feed rate and screw speed is shown in Fig. 9.

L/S ratio had a larger effect on granule porosity (a in Fig. 9) compared to screw speed and mass feed ratio, which agrees with the findings of previous research (Verstraeten et al., 2017).

Mass feed rate did not have an effect on granule porosity for formulation 2R50 as shown by the granule porosity at low and high mass feed rate at each compartment lying close to each other (b in Fig. 9).

The effect of screw speed on granule porosity for formulation 2R50 is shown in Fig. 9 - c. The final porosity (C6) of size fractions 850 – 1000 µm and >2000 µm decreased with decreasing screw speed. This was caused by the reduction in granule porosity in KZ2 (C3 to C5) when applying a low screw speed. There are a few possible explanations for this effect. First, the longer residence time of the granules inside the TSG at low screw speed could increase the opportunity of inter-granular collisions and hence consolidation in KZ2. Second, granules are less likely to break into smaller particles when a lower amount of shear is applied (i.e., when using a lower screw speed). Instead, the initial granules will be sheared and compressed by the kneading elements in KZ2. Third, there could be more granule consolidation in KZ2 at low

screw speed because of the higher barrel fill level, which causes more inter-granular collisions. Yet, this is an unlikely reason for the effect of screw speed on granule porosity because in that case, changing the mass feed rate would also influence the granule porosity by its effect on the barrel fill level.

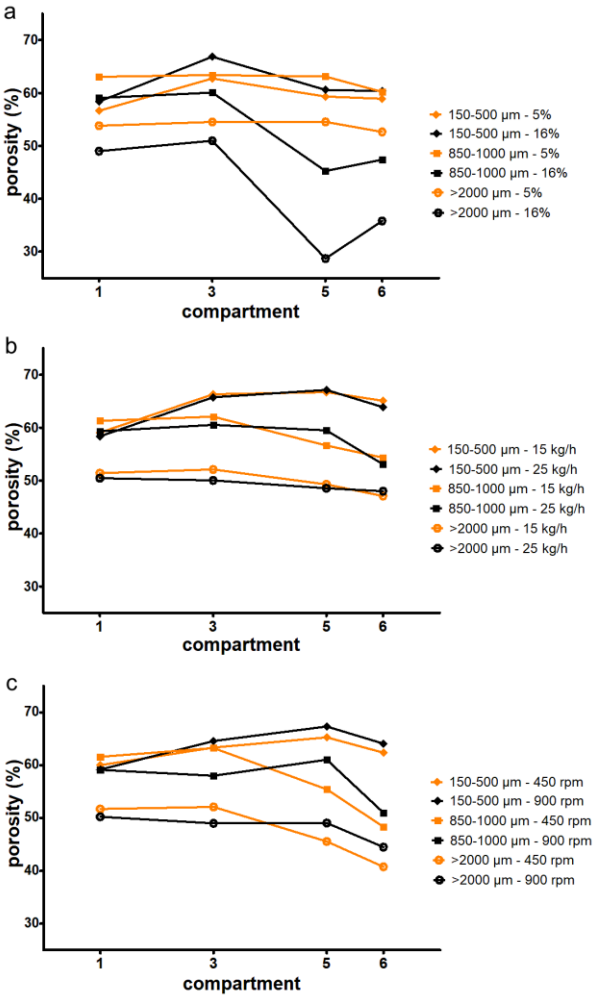

Fig. 9. Granule porosity at the intermediate TSG compartments for 2R50 applying low and high (a) L/S ratio, (b) mass feed rate and (c) screw speed.

5. Conclusion

This study investigated the effect of raw material properties, twin-screw wet granulation process parameters, and screw elements on granule porosity.

Several water-related properties (e.g., solubility (S_{max}), dissolution rate (DR)), particle size (e.g., d50_w), density (e.g., ρb) and flow properties (e.g., ffc) of the API were found to have an important effect on granule porosity. The water-related material properties were more important for granule porosity at the downstream TSG compartments (i.e., C5 and C6) whereas other properties such as particle size were equally important in the upstream compartments (i.e., C1 and C3). The effect of these raw material properties upon granule porosity was also influenced by the applied L/S ratio. Water-related properties were dominant at a high L/S ratio whereas particle size and flow properties were most important when applying a low L/S ratio.

While the L/S ratio was confirmed to be the dictating process parameter, granulator screw speed was also found to be an important process parameter affecting granule porosity.

This study yielded valuable information on the key parameters affecting granule porosity which can be used for TSWG process and formulation development. Furthermore, this information is crucial to develop predictive mechanistic models such as multi-dimensional PBMs (Barrera Jiménez et al., 2023b). More studies on experimental variabilities, e.g., deviations of porosity, would improve the accuracy of these mechanistic models. In a follow-up study, the effect of different excipients and varying drug loads on porosity could be evaluated. Also collecting data for APIs with different physical-chemical properties would allow to develop models with a wider applicability. Since the development of population balance models requires granule porosity distribution information, the current dataset could be expanded by measuring the granule porosity of the studied formulations for additional size fractions.

CRediT authorship contribution statement

Michiel Peeters: Conceptualization, Methodology, Validation, Formal analysis, Investigation, Data curation, Writing – original draft, Writing – review & editing, Visualization, Project administration. **Ana Alejandra Barrera Jimenez:** Conceptualization, Methodology, Writing – review & editing. **Kensaku Matsunami**: Conceptualization, Methodology, Writing – original draft, Writing – review & editing. **Fanny Stauffer**: writing – review & editing, funding. **Ingmar Nopens:** Conceptualization, Resources, Writing – review & editing, Supervision, Project administration, Funding acquisition. **Thomas De Beer:** Conceptualization, Resources, Writing – original draft, Writing – review & editing, Supervision, Project administration, Funding acquisition.

Acknowledgements

The authors would like to thank UCB for funding this study and for the fruitful collaboration in this project.

6. References

Ansari, M.A., Stepanek, F., 2008. The effect of granule microstructure on dissolution rate. Powder Technol. 181, 104–114. https://doi.org/10.1016/J.POWTEC.2006.12.012

Badawy, S.I.F., Menning, M.M., Gorko, M.A., Gilbert, D.L., 2000. Effect of process parameters on compressibility of granulation manufactured in a high-shear mixer. Int. J. Pharm. 198, 51–61. https://doi.org/10.1016/S0378-5173(99)00445-7

Badawy, S.I.F., Narang, A.S., Lamarche, K., Subramanian, G., Varia, S.A., 2012. Mechanistic basis for the effects of process parameters on quality attributes in high shear wet granulation. Int. J. Pharm. 439, 324–333. https://doi.org/10.1016/J.IJPHARM.2012.09.011

Barrasso, D., El Hagrasy, A., Litster, J.D., Ramachandran, R., 2015. Multi-dimensional population balance model development and validation for a twin screw granulation process. Powder Technol. 270, 612–621. https://doi.org/10.1016/J.POWTEC.2014.06.035

Barrasso, D., Ramachandran, R., 2016. Qualitative Assessment of a Multi-Scale, Compartmental PBM-DEM Model of a Continuous Twin-Screw Wet Granulation Process. J. Pharm. Innov. 11, 231–249. https://doi.org/10.1007/S12247-015-9240-7/FIGURES/11

Barrasso, D., Walia, S., Ramachandran, R., 2013. Multi-component population balance modeling of continuous granulation processes: A parametric study and comparison with experimental trends. Powder Technol. 241, 85–97. https://doi.org/10.1016/J.POWTEC.2013.03.001

Barrera Jiménez, A.A., Van Hauwermeiren, D., Peeters, M., De Beer, T., Nopens, I., 2021. Improvement of a 1D Population Balance Model for Twin-Screw Wet Granulation by Using Identifiability Analysis. Pharm. 2021, Vol. 13, Page 692 13, 692. https://doi.org/10.3390/PHARMACEUTICS13050692

Beer, P., Wilson, D., Huang, Z., De Matas, M., 2014. Transfer from high-shear batch to continuous twin screw wet granulation: A case study in understanding the relationship between process parameters and product quality attributes. J. Pharm. Sci. 103, 3075–3082. https://doi.org/10.1002/JPS.24078

Dhenge, R.M., Cartwright, J.J., Doughty, D.G., Hounslow, M.J., Salman, A.D., 2011. Twin screw wet granulation: Effect of powder feed rate. Adv. Powder Technol. https://doi.org/10.1016/j.apt.2010.09.004

Dhenge, R.M., Cartwright, J.J., Hounslow, M.J., Salman, A.D., 2012. Twin screw wet granulation: Effects of properties of granulation liquid. Powder Technol. 229, 126–136. https://doi.org/10.1016/J.POWTEC.2012.06.019

Dhenge, R.M., Fyles, R.S., Cartwright, J.J., Doughty, D.G., Hounslow, M.J., Salman, A.D., 2010. Twin screw wet granulation: Granule properties. Chem. Eng. J. https://doi.org/10.1016/j.cej.2010.05.023

El Hagrasy, A.S., Hennenkamp, J.R., Burke, M.D., Cartwright, J.J., Litster, J.D., 2013. Twin screw wet granulation: Influence of formulation parameters on granule properties and growth behavior. Powder Technol. 238, 108–115. https://doi.org/10.1016/J.POWTEC.2012.04.035

El Hagrasy, A.S., Litster, J.D., 2013. Granulation rate processes in the kneading elements of a twin screw granulator. AIChE J. 59, 4100–4115. https://doi.org/10.1002/AIC.14180

Fonteyne, M., Correia, A., De Plecker, S., Vercruysse, J., Ilić, I., Zhou, Q., Vervaet, C., Remon, J.P., Onofre, F., Bulone, V., De Beer, T., 2015. Impact of microcrystalline

cellulose material attributes: A case study on continuous twin screw granulation. Int. J. Pharm. 478. https://doi.org/10.1016/j.ijpharm.2014.11.070

Fonteyne, M., Vercruysse, J., Díaz, D.C., Gildemyn, D., Vervaet, C., Remon, J.P., Beer, T. De, 2013. Real-time assessment of critical quality attributes of a continuous granulation process. Pharm. Dev. Technol. 18, 85–97. https://doi.org/10.3109/10837450.2011.627869

Immanuel, C.D., Doyle, F.J., 2005. Solution technique for a multi-dimensional population balance model describing granulation processes. Powder Technol. 156, 213–225. https://doi.org/10.1016/J.POWTEC.2005.04.013

Ismail, H.Y., Singh, M., Albadarin, A.B., Walker, G.M., 2020. Complete two dimensional population balance modelling of wet granulation in twin screw. Int. J. Pharm. 591, 120018. https://doi.org/10.1016/J.IJPHARM.2020.120018

Ismail, H.Y., Singh, M., Darwish, S., Kuhs, M., Shirazian, S., Croker, D.M., Khraisheh, M., Albadarin, A.B., Walker, G.M., 2019. Developing ANN-Kriging hybrid model based on process parameters for prediction of mean residence time distribution in twin-screw wet granulation. Powder Technol. 343, 568–577. https://doi.org/10.1016/J.POWTEC.2018.11.060

Iveson, S.M., Litster, J.D., 1998. Fundamental studies of granule consolidation. Part 2: Quantifying the effects of particle and binder properties. Powder Technol. 99, 243–250. https://doi.org/10.1016/S0032-5910(98)00116-8

Iveson, S.M., Litster, J.D., Ermis, B.J., 1996. Fundamental studies of granule consolidation Part 1: Effects of binder content and binder viscosity. Powder Technol. 88, 15–20.

Kumar, A., Vercruysse, J., Mortier, S.T.F.C., Vervaet, C., Remon, J.P., Gernaey, K. V., De Beer, T., Nopens, I., 2016. Model-based analysis of a twin-screw wet granulation system for continuous solid dosage manufacturing. Comput. Chem. Eng. 89, 62–70. https://doi.org/10.1016/J.COMPCHEMENG.2016.03.007

Lee, S.L., O'Connor, T.F., Yang, X., Cruz, C.N., Chatterjee, S., Madurawe, R.D., Moore, C.M.V., Yu, L.X., Woodcock, J., 2015. Modernizing Pharmaceutical Manufacturing: from Batch to Continuous Production. J. Pharm. Innov. https://doi.org/10.1007/s12247-015-9215-8

Li, H., Thompson, M.R., O'Donnell, K.P., 2014. Understanding wet granulation in the kneading block of twin screw extruders. Chem. Eng. Sci. 113, 11–21. https://doi.org/10.1016/J.CES.2014.03.007

Liu, H., Galbraith, S.C., Park, S.Y., Cha, B., Huang, Z., Meyer, R.F., Flamm, M.H., O'Connor, T., Lee, S., Yoon, S., 2018. Assessment of spatial heterogeneity in continuous twin screw wet granulation process using three-compartmental population balance model. https://doi.org/10.1080/10837450.2018.1427106 24, 105–117. https://doi.org/10.1080/10837450.2018.1427106

Meier, R., Moll, K.P., Krumme, M., Kleinebudde, P., 2017. Impact of fill-level in twin-screw granulation on critical quality attributes of granules and tablets. Eur. J. Pharm. Biopharm. 115. https://doi.org/10.1016/j.ejpb.2017.02.010

Meng, W., Rao, K.S., Snee, R.D., Ramachandran, R., Muzzio, F.J., 2019. A comprehensive analysis and optimization of continuous twin-screw granulation processes via sequential experimentation strategy. Int. J. Pharm. 556, 349–362. https://doi.org/10.1016/J.IJPHARM.2018.12.009

Narang, A.S., Badawy, S.I.F. (Eds.), 2019. Handbook Of Pharmaceutical Wet Granulation, Handbook of Pharmaceutical Wet Granulation. Academic Press.

https://doi.org/10.1016/b978-0-12-810460-6.09991-7

Nordström, J., Alderborn, G., 2015. The Granule Porosity Controls the Loss of Compactibility for Both Dry- and Wet-Processed Cellulose Granules but at Different Rate. J. Pharm. Sci. 104, 2029–2039. https://doi.org/10.1002/JPS.24439

Osorio, J.G., Sayin, R., Kalbag, A. V., Litster, J.D., Martinez-Marcos, L., Lamprou, D.A., Halbert, G.W., 2017. Scaling of continuous twin screw wet granulation. AIChE J. 63, 921–932. https://doi.org/10.1002/AIC.15459

Pandey, P., Tao, J., Chaudhury, A., Ramachandran, R., Gao, J.Z., Bindra, D.S., 2012. A combined experimental and modeling approach to study the effects of high-shear wet granulation process parameters on granule characteristics. https://doi.org/10.3109/10837450.2012.700933 18, 210–224. https://doi.org/10.3109/10837450.2012.700933

Poon, J.M.H., Immanuel, C.D., Doyle, F.J., Litster, J.D., 2008. A three-dimensional population balance model of granulation with a mechanistic representation of the nucleation and aggregation phenomena. Chem. Eng. Sci. 63, 1315–1329. https://doi.org/10.1016/J.CES.2007.07.048

Portier, C., Pandelaere, K., Delaet, U., Vigh, T., Di Pretoro, G., De Beer, T., Vervaet, C., Vanhoorne, V., 2020a. Continuous twin screw granulation: A complex interplay between formulation properties, process settings and screw design. Int. J. Pharm. 576, 119004. https://doi.org/10.1016/j.ijpharm.2019.119004

Portier, C., Pandelaere, K., Delaet, U., Vigh, T., Kumar, A., Di Pretoro, G., De Beer, T., Vervaet, C., Vanhoorne, V., 2020b. Continuous twin screw granulation: Influence of process and formulation variables on granule quality attributes of model formulations. Int. J. Pharm. 576, 118981. https://doi.org/10.1016/j.ijpharm.2019.118981

Portier, C., Vervaet, C., Vanhoorne, V., 2021. Continuous Twin Screw Granulation: A Review of Recent Progress and Opportunities in Formulation and Equipment Design. Pharm. 2021, Vol. 13, Page 668 13, 668. https://doi.org/10.3390/PHARMACEUTICS13050668

Rantanen, J., Khinast, J., 2015. The Future of Pharmaceutical Manufacturing Sciences. J. Pharm. Sci. 104, 3612–3638. https://doi.org/10.1002/JPS.24594

Ryckaert, A., Van Hauwermeiren, D., Dhondt, J., De Man, A., Funke, A., Djuric, D., Vervaet, C., Nopens, I., De Beer, T., 2021. TPLS as predictive platform for twin-screw wet granulation process and formulation development. Int. J. Pharm. 605, 120785. https://doi.org/10.1016/J.IJPHARM.2021.120785

Seem, T.C., Rowson, N.A., Ingram, A., Huang, Z., Yu, S., de Matas, M., Gabbott, I., Reynolds, G.K., 2015. Twin screw granulation - A literature review. Powder Technol. https://doi.org/10.1016/j.powtec.2015.01.075

Shirazian, S., Ismail, H.Y., Singh, M., Shaikh, R., Croker, D.M., Walker, G.M., 2019. Multi-dimensional population balance modelling of pharmaceutical formulations for continuous twin-screw wet granulation: Determination of liquid distribution. Int. J. Pharm. 566, 352–360. https://doi.org/10.1016/J.IJPHARM.2019.06.001

Stauffer, F., Vanhoorne, V., Pilcer, G., Chavez, P.F., Vervaet, C., De Beer, T., 2019. Managing API raw material variability during continuous twin-screw wet granulation. Int. J. Pharm. 561. https://doi.org/10.1016/j.ijpharm.2019.03.012

Thompson, M.R., Sun, J., 2010. Wet Granulation in a Twin-Screw Extruder: Implications of Screw Design. J. Pharm. Sci. 99, 2090–2103. https://doi.org/10.1002/JPS.21973

Van Hauwermeiren, D., Stock, M., De Beer, T., Nopens, I., 2020. Predicting Pharmaceutical

Particle Size Distributions Using Kernel Mean Embedding. Pharm. 2020, Vol. 12, Page 271 12, 271. https://doi.org/10.3390/PHARMACEUTICS12030271

Van Hauwermeiren, D., Verstraeten, M., Doshi, P., am Ende, M.T., Turnbull, N., Lee, K., De Beer, T., Nopens, I., 2018. On the modelling of granule size distributions in twin-screw wet granulation: Calibration of a novel compartmental population balance model. Powder Technol. 341, 116–125. https://doi.org/10.1016/j.powtec.2018.05.025

Vanhoorne, V., Vanbillemont, B., Vercruysse, J., De Leersnyder, F., Gomes, P., De Beer, T., Remon, J.P., Vervaet, C., 2016. Development of a controlled release formulation by continuous twin screw granulation: Influence of process and formulation parameters. Int. J. Pharm. 505. https://doi.org/10.1016/j.ijpharm.2016.03.058

Vanhoorne, V., Vervaet, C., 2020. Recent progress in continuous manufacturing of oral solid dosage forms. Int. J. Pharm. 579, 119194. https://doi.org/10.1016/j.ijpharm.2020.119194

Vercruysse, J., Burggraeve, A., Fonteyne, M., Cappuyns, P., Delaet, U., Van Assche, I., De Beer, T., Remon, J.P., Vervaet, C., 2015. Impact of screw configuration on the particle size distribution of granules produced by twin screw granulation. Int. J. Pharm. 479. https://doi.org/10.1016/j.ijpharm.2014.12.071

Vercruysse, J., Córdoba Díaz, D., Peeters, E., Fonteyne, M., Delaet, U., Van Assche, I., De Beer, T., Remon, J.P., Vervaet, C., 2012. Continuous twin screw granulation: Influence of process variables on granule and tablet quality. Eur. J. Pharm. Biopharm. 82, 205–211. https://doi.org/10.1016/j.ejpb.2012.05.010

Verstraeten, M., Van Hauwermeiren, D., Lee, K., Turnbull, N., Wilsdon, D., am Ende, M., Doshi, P., Vervaet, C., Brouckaert, D., Mortier, S.T.F.C., Nopens, I., Beer, T. De, 2017. In-depth experimental analysis of pharmaceutical twin-screw wet granulation in view of detailed process understanding. Int. J. Pharm. 529, 678–693. https://doi.org/10.1016/j.ijpharm.2017.07.045

Wang, L.G., Pradhan, S.U., Wassgren, C., Barrasso, D., Slade, D., Litster, J.D., 2020. A breakage kernel for use in population balance modelling of twin screw granulation. Powder Technol. 363, 525–540. https://doi.org/10.1016/J.POWTEC.2020.01.024

Webb, P.A., 2001. Volume and Density Determinations for Particle Technologists.